AGU ADVANCING EARTH AND SPACE SCIENCE

Water Resources Research

RESEARCH ARTICLE
10.1029/2021WR030333

Impact of Coastal Marsh Eco-Geomorphologic Change on Saltwater Intrusion Under Future Sea Level Rise

Yu Zhang[1], Daniil Svyatsky[2], Joel C. Rowland[1], J. David Moulton[2], Zhendong Cao[2,3], Phillip J. Wolfram[4], Chonggang Xu[1], and Donatella Pasqualini[5]

[1]Earth and Environmental Sciences Division,, Los Alamos National Laboratory, Los Alamos, NM, USA, [2]Theoretical Division, Los Alamos National Laboratory, Los Alamos, NM, USA, [3]Center for Applied Coastal Research, University of Delaware, Newark, DE, USA, [4]Advanced Engineering Analysis, Los Alamos National Laboratory, Los Alamos, NM, USA, [5]Analytics, Intelligence & Technology Division, Los Alamos National Laboratory, Los Alamos, NM, USA

Key Points:

- The effect of coastal marsh evolution on future saltwater intrusion is examined for the first time
- Marsh accretion under sea level rise may significantly reduce surface seawater inflow and prolong the surface seawater residence time
- Future saltwater intrusion on the evolved marsh landscape may become more sensitive to upland groundwater inflows

Supporting Information:

Supporting Information may be found in the online version of this article.

Correspondence to:

Y. Zhang,
yuzhang@lanl.gov

Citation:

Zhang, Y., Svyatsky, D., Rowland, J. C., Moulton, J. D., Cao, Z., Wolfram, P. J., et al. (2022). Impact of coastal marsh eco-geomorphologic change on saltwater intrusion under future sea level rise. *Water Resources Research*, *58*, e2021WR030333. https://doi.org/10.1029/2021WR030333

Received 30 APR 2021
Accepted 8 MAY 2022

Author Contributions:

Conceptualization: Yu Zhang
Data curation: Yu Zhang
Formal analysis: Yu Zhang, Daniil Svyatsky, Chonggang Xu
Investigation: Yu Zhang
Methodology: Yu Zhang, Joel C. Rowland, J. David Moulton, Zhendong Cao
Project Administration: Joel C. Rowland, J. David Moulton, Donatella Pasqualini
Resources: Yu Zhang
Software: Yu Zhang, Daniil Svyatsky, J. David Moulton

Abstract Coastal saltwater intrusion (SWI) is one key factor that affects the hydrology, ecology, and biogeochemistry of coastal ecosystems. Future climate change, especially intensified sea level rise (SLR), is expected to trigger SWI to encroach on coastal freshwater aquifers more intensively. Numerous studies have investigated decadal/century scale SWI under SLR by assuming a static coastal landscape topography. However, coastal landscapes are highly dynamic in response to SLR, and the impact of coastal landscape evolution on SWI has received very little attention. Thus, this study used a coastal marsh landscape as an example and investigated how coastal marsh evolution affects future SWI with a physically-based coastal hydro-eco-geomorphologic model, Advanced Terrestrial Simulator. Our numerical experiments showed that it is very likely that the marsh elevation increases with future SLR due to sediment deposition, and a depression zone is formed due to different marsh accretion rates between the ocean boundary and the inland. We found that marsh accretion may significantly reduce the surface saltwater inflow at the ocean boundary, and the evolved topographic depression zone may prolong the residence time of surface ponded saltwater, affecting subsurface salinity distribution differently. We also predicted that marshlands may become more sensitive to upland freshwater supply under future SLR, compared with previous predictions without marsh evolution. This study demonstrates the importance of coastal evolution to coastal freshwater-saltwater interaction. The eco-geomorphologic effect may not be ignored when evaluating coastal SWI under SLR at decadal or century scales.

1. Introduction

Coastal wetlands, unique landscapes that connect the terrestrial landscape and the ocean, are some of the most productive ecosystems on Earth (Tiner, 2013). Climate change, especially sea level rise (SLR) under a warming climate, is one of the biggest threats to the stability and sustainability of coastal wetland ecosystems (Burkett & Kusler, 2000). SLR-driven impacts on coastal marsh ecosystems are strongly affected by changes in coastal hydrology (Zhang et al., 2019). The rising sea level alters the balance of coastal freshwater-saltwater interaction both on the coastal wetland surface and in the subsurface aquifer causing the changes in saltwater intrusion (SWI), thereby affecting soil water salinity (Guimond & Tamborski, 2021; Sorensen et al., 1984; Sousa et al., 2010), triggering the mortality of salt-intolerant vegetation (Silvestri & Marani, 2004), and eventually altering the ecosystem functions of coastal wetlands (Burkett & Kusler, 2000). Therefore, investigating the response of SWI to SLR is critical for our understanding of the SLR impact on coastal wetland ecosystems.

Numerous studies have attempted to predict and/or assess the impact of SLR on SWI for decades. These studies have aimed to track the changes in water salinity in coastal aquifers driven by SLR at global (e.g., Ferguson & Gleeson, 2012; Michael et al., 2013), regional (e.g., Oude Essink et al., 2010; Zhang et al., 2018, 2019), and local/transect scales (e.g., Ataie-Ashtiani et al., 2013; Carretero et al., 2013; Chang et al., 2011; Chen et al., 2015; Giambastiani et al., 2007; Hughes et al., 2009; Ketabchi et al., 2014; Langevin & Zygnerski, 2013; Loáiciga et al., 2012; Lu et al., 2015; Masterson & Garabedian, 2007; Mazi et al., 2013; Morgan et al., 2013; Payne, 2010; Rasmussen et al., 2013; Sefelnasr & Sherif, 2014; Vandenbohede et al., 2008; Vu et al., 2018; Werner & Simmons, 2009; Yang et al., 2015). By using analytical or numerical models, these studies examined SWI in coastal aquifers under SLR, especially under the influence of different environmental settings, such as regional-scale hydrologic connectivity, upland groundwater boundary condition, and land surface inundation, groundwater extraction, and

Supervision: Joel C. Rowland, J. David Moulton, Phillip J. Wolfram, Chonggang Xu, Donatella Pasqualini
Validation: Yu Zhang, Daniil Svyatsky
Visualization: Yu Zhang
Writing – original draft: Yu Zhang, Daniil Svyatsky, Joel C. Rowland, J. David Moulton, Zhendong Cao, Phillip J. Wolfram, Chonggang Xu, Donatella Pasqualini

recharge. For example, Zhang et al. (2018, 2019) investigated the groundwater flow path and SWI of the coastal wetlands in North Carolina, USA, by considering regional-scale coastal hydrologic connectivity. They found that aquifers with the largest seasonal changes of SWI are located hundreds of meters away from the shoreline, where freshwater strongly interacts with saltwater. In terms of the effect of upland boundary conditions on SWI, upland boundary conditions may control the freshwater and saltwater interaction differently, such as (a) the flux-controlled boundary condition, where fresh groundwater flux to the ocean is persistent despite how sea level would change and (b) the head-controlled boundary condition, where the upland climate and/or the connection with surface water bodies (e.g., lakes and rivers) maintain a stable water head condition regardless the changes in sea level. For example, Werner and Simmons (2009) and Werner et al. (2012) found that SLR impact is more extensive in unconfined aquifers with a groundwater head-controlled inland boundary, compared with confined aquifers. Carretero et al. (2013) found that SWI increased linearly with SLR in aquifers with a flux-controlled boundary condition, but increased nonlinearly with a head-controlled boundary condition. In terms of the effect of groundwater extraction and freshwater supply (recharge), Loáiciga et al. (2012) found that groundwater extraction was the predominant driver of SWI in one coastal aquifer in Monterey, California, compared with the effect of SLR. Using another coastal aquifer in the Western Baltic Sea as an example, Rasmussen et al. (2013) found that the SWI in flux-controlled aquifers is more sensitive to recharge than SLR. Likewise, Ataie-Ashtiani et al. (2013) found that surface inundation may induce significantly more extensive SWI than SLR. Each of these studies provided insights into understanding SWI under SLR in the temporal scales of decades and centuries, however, none of them considered the effect of coastal landscape topographic change. Understanding this effect is particularly important for coastal wetlands because (a) coastal wetlands (especially coastal marsh) are geomorphologically dynamic systems in response to sediment erosion/deposition driven by tide, SLR, and vegetation productivity (Fagherazzi et al., 2013) and (b) the topographic change may have a significant impact on SWI by altering saltwater flow paths and residence time, thereby changing the surface and subsurface salinity and affecting salt-tolerant and salt-intolerant vegetation redistribution, colonization, and ecosystem functions (Silvestri & Marani, 2004).

The landscape evolution of coastal wetlands under SLR has been explored extensively by the coastal geomorphologic community. Many studies have predicted coastal marsh evolution as a function of sediment erosion and deposition and organic soil production due to vegetation productivity. They found that coastal marshes are not static and are very likely to keep pace with the rising sea level at decadal to century scales due to the net sedimentation on the marshlands (e.g., Best et al., 2018; D'Alpaos et al., 2007; Kirwan, Temmerman, et al., 2016; Kirwan, Walters, et al., 2016; Kirwan & Murray, 2007; Kirwan & Temmerman, 2009; Mariotti & Fagherazzi, 2010; Zhang et al., 2020). With the changes in marsh geomorphology, the topographic and hydraulic gradient among the land, river, and ocean will change, which will alter the seawater flow path and storage (Winn et al., 2006). However, so far, there is a critical knowledge gap on how the evolution of coastal landscape may affect SWI under SLR. This could severely limit our capability to accurately estimate the vulnerability of coastal aquifers to SWI under SLR. To fill this knowledge gap, in this study, we used synthetic numerical experiments to examine the effect of coastal marsh evolution on coastal SWI under SLR. We simulated coastal marsh evolution and SWI on synthetic coastal marsh transects under different rates of SLR over 100 years by using the coastal marsh evolution model and a density-dependent solute transport model in the Advanced Terrestrial Simulator (ATS) (Coon et al., 2016). We evaluated the impact of coastal marsh evolution on SWI by comparing the surface and subsurface hydrologic characteristics of the SWI simulations with and without considering coastal marsh evolution. The surface hydrologic characteristics include seawater propagation, seawater inflow rate, surface salt concentration, and surface seawater infiltration. The subsurface hydrologic characteristics include subsurface water salinity distribution, seawater inflow, and the displacement of the freshwater-saltwater interface. We hypothesized that coastal marsh evolution cannot be ignored when evaluating coastal SWI under SLR at a decadal or century scale because the evolved surface topography may significantly affect surface seawater inflow rate and surface water residence time, therefore changing SWI. The insights gained from this study can help improve our understanding of the vulnerability of coastal freshwater systems to SWI.

In this study, we first introduce the numerical model, experiment and scenario designs, and evaluation metrics in Section 2, after which we present and analyze the results from the numerical experiments for marsh evolution and SWI in Section 3. Lastly, Section 4 discusses the implication of this study for understanding SWI under SLR from a coupled hydro-eco-geomorphologic framework, its representativeness, uncertainties, and outlined future work, followed by conclusions in Section 5.

2. Materials and Methods

2.1. Mathematical Models

This study used the Advanced Terrestrial Simulator (ATS) (Coon et al., 2016) to simulate SWI and coastal marsh evolution under future SLR. ATS is a multi-process high-performance computing simulator with process kernels (PKs) for surface and subsurface hydrology, energy balance, thermal dynamics, sediment transport, solute transport, coastal marsh evolution, and marsh vegetation dynamics. Here we used some ATS PKs to configure a saltwater intrusion model and a coastal marsh evolution model.

2.1.1. The Configuration of Coastal Saltwater Intrusion in ATS

We used the SWI configuration in ATS (hereinafter referred to as the SWI model) to simulate the salinity change of surface and subsurface water by coupling surface and subsurface hydrologic processes with density-dependent solute transport processes. The integrated hydrologic processes include a two-dimensional (2-D) diffusive-wave approximation of surface flows (Vreugdenhil, 1994) and a variably saturated three-dimensional (3-D) Richards equation (Richards, 1931) for subsurface flows. The governing system of PDEs for surface and subsurface fluid mass balance is as follows,

$$\begin{cases} \dfrac{\partial d\rho_1}{\partial t} = -\nabla_1 (\rho_1 d\mathrm{u}) - I_w \\ \dfrac{\partial \theta\sigma\rho_2}{\partial t} = -\nabla_2 (\rho_2 q) + I_w \end{cases} \tag{1}$$

where $\rho_1(C_1)$ and $\rho_2(C_2)$ are the surface and subsurface fluid density (kg/m^3) which are functions of surface and subsurface salt concentrations (dimensionless), C_1 and C_2, respectively; d is the surface water depth (m); θ is the subsurface water content; σ is the soil porosity; I_w is the mass source/sink term (kg/s m^2) representing the infiltration or exfiltration (positive in the downward direction); u is the depth-averaged surface flow velocity (m/s) which is, according to the diffusive wave approximation, defined as follows:

$$\mathrm{u} = -\frac{d^{\frac{2}{3}}}{n(max(|\nabla(z+d)|,\epsilon))^{\frac{1}{2}}} \nabla(z+d) \tag{2}$$

where z is the surface elevation (m); n is the Manning's coefficient of roughness ($s/m^{1/3}$); the coefficient, ε>0, is used to regularize the surface velocity when the bed slope is 0; q in Equation 1 is the subsurface water flow velocity (m/s) defined by Darcy law:

$$q = -\frac{k_r K}{\mu} \nabla h \tag{3}$$

where k_r and K are a relative (dimensionless) and absolute permeabilities (m^2), respectively, μ is fluid dynamic viscosity (kg/m/s) and h is subsurface water pressure (Pa, or N/m^2, or kg/m/s^2).

In Equation 1, the density is a linear function of water concentration (Simmons et al., 2001):

$$\rho = \rho_0 + a(C - C_0) \tag{4}$$

where ρ is the fluid density for surface water or subsurface water (kg/m^3); C is the fluid salt concentration for surface and subsurface water (dimensionless); ρ_0 is the fluid density at a base concentration, C_0; a is a constant coefficient of density variability.

The generic form of saltwater concentration is calculated based on the salt mass balance equation following Herbert et al. (1988) and Simmons et al. (2001).

$$\begin{cases} \dfrac{\partial (d\rho_1 C_1)}{\partial t} = -\nabla_1 (d\rho_1 u C_1) + \nabla_1 [d\rho_1 (D_0 + D) \cdot \nabla_1 C_1] - \mathrm{I}_{\mathrm{salt}} \\ \dfrac{\partial (\theta\sigma\rho_2 C_2)}{\partial t} = -\nabla_2 (\theta\sigma\rho_2 q C_2) + \nabla_2 [\theta\sigma\rho_2 (D_0 + D) \cdot \nabla_2 C_2] + \mathrm{I}_{\mathrm{salt}} \end{cases} \tag{5}$$

where C_1 and C_2 are the salt concentration of surface and subsurface water (dimensionless), respectively. D_0 is the molecular diffusivity (m^2/s). $\boldsymbol{D}$ is the transverse and longitudinal dispersivities; Likewise, I_{salt} is the mass source/

sink term (kg/s m^2) representing the infiltration or exfiltration (positive in the downward direction). The capability of the SWI model in capturing saltwater intrusion through surface and subsurface flow under tidal conditions was validated by comparing the model simulation with a lab experiment of SWI with tidal variation by Kuan et al. (2019). The simulated freshwater-saltwater interface agreed with the lab experiment well (see the validation results in the supplementary information Text S1 and Figures S1 and S2).

2.1.2. The Configuration of Coastal Marsh Evolution in ATS

For the marsh evolution modeling, we used the coastal marsh evolution model (hereinafter referred to as Sed model) configured by the 2-D surface flow, sediment transport and marsh evolution PKs in ATS. The Sed model tracks the change of marsh surface elevation as a function of sediment erosion, sediment settling, sediment trapping by vegetation, and vegetation organic matter production. Namely,

$$\frac{dz}{dt} = \frac{1}{\rho_s}(D_s + D_t - E) + D_{org} \tag{6}$$

where z is the surface elevation (m); t is the time (s); ρ_s is the sediment bulk density (kg/m^3); D_s is the inorganic sediment settling rate (kg/m^2/s); D_t is the inorganic sediment trapping rate due to the effect of vegetation canopy (kg/m^2/s); E represents local sediment erosion rate (kg/m^2/s); D_{org} is the organic matter production rate (m/s).

The Sed model follows the forms of sediment erosion and deposition in D'Alpaos et al. (2007), but improved the representation of surface hydrodynamics, instead of using an equilibrium assumption for surface hydrodynamics. Specifically, in the Sed model, the surface hydrodynamics due to tide and SLR is represented by a depth-averaged diffusive-wave scheme (Equation 2) considering the spatial and temporal variations of water propagation landward. Sediment erosion (E in Equation 6) is estimated as a linear function of dynamic bed shear stress depending on surface water flow velocity. Erosion occurs when the bed shear stress due to water flow (τ_0) is greater than the critical shear stress for erosion (τ_e). Namely,

$$E = \begin{cases} \alpha\left(\frac{\tau_0}{\tau_e} - 1\right) & if\ \tau_0 > \tau_e \\ 0 & if\ \tau_0 < \tau_e \end{cases} \tag{7}$$

where α is the erosion coefficient. Likewise, sediment settling (D_s in Equation 6) describes the process which particulates settle to the bottom of a liquid and form sediment due to gravity, which is also assumed as a linear function of dynamic bed shear stress. Sediment settling occurs when the bed shear stress (τ_0) is smaller than the critical shear stress for deposition (τ_d), viz

$$D_s = \begin{cases} w_s C_s\left(1 - \frac{\tau_0}{\tau_d}\right) & if\ \tau_0 < \tau_d \\ 0 & if\ \tau_0 > \tau_d \end{cases} \tag{8}$$

where w_s is the settling velocity (m/s); C_s is the suspended sediment concentration (kg/m^3). Sediment trapping by vegetation (D_t in Equation 6) is given by

$$D_t = C_s U \epsilon d_s n_s \min[h_s, h_w] \tag{9}$$

where D_t is a function of water flow velocity (U), a capture efficiency of vegetation stems (ϵ), water depth (h_w), and several vegetation characteristics, such as plant stem diameter (d_s), stem density (n_s), and vegetation height (h_s). The vegetation properties are determined by vegetation biomass, which is assumed as a linear function of marsh surface elevation relative to the mean highest tide level. Also, the vegetation organic matter production (D_{org} in Equation 6) is a linear function of vegetation biomass, viz

$$D_{org} = K_b \frac{B}{B_{max}} \tag{10}$$

where K_b is the maximum production rate of belowground organic material [m/s]; B is the aboveground plant dry biomass at the current time [g/m^2]; and B_{max} is the maximum vegetation biomass [g/m^2]. Most of the current coastal marsh biomass predictions are based on the field measurements from Morris et al. (2002). In this study,

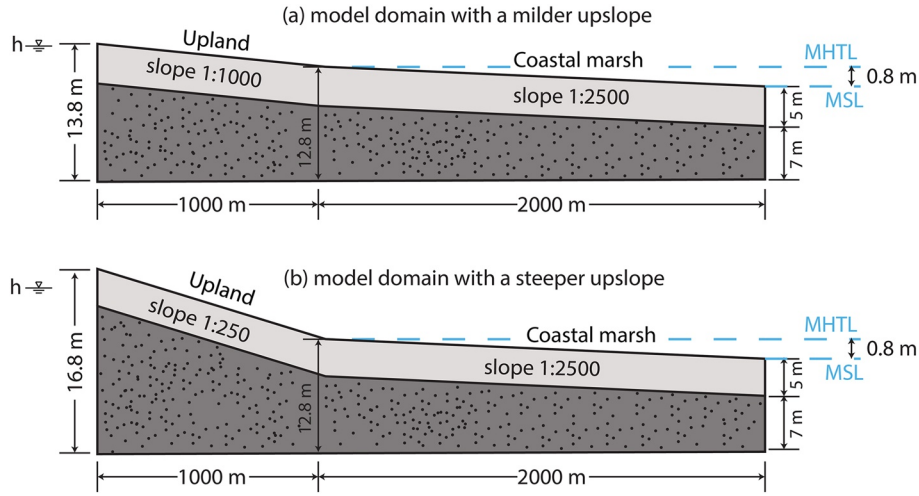

Figure 1. Sketches of the 2-D model domain with a low permeable upper layer (light gray color) and a high permeable bottom layer (dark gray color with black dots). The surface elevation at the ocean boundary (right side) is 0 m. The elevation at the upland boundary is 1.8 m for the milder upslope domain and 4.8 m for the steeper upslope domain. MHTL stands for the mean highest tide level and MSL is the mean sea level. The present-day MSL is at the 0 m level. h at the left side of the domain indicates the upland groundwater level. Three upland groundwater level scenarios are used: $h = 1.3$ m (present-day level), $h = 1.8$ (reflecting future wetter climate), and $h = 0.9$ m (reflecting future drier climate or more groundwater extraction).

we assume that the aboveground biomass of the salt-tolerant marsh vegetation increases linearly with the inundation level, same as many previous marsh evolution studies (e.g., Belliard et al., 2015; D'Alpaos et al., 2007). Some studies also quantified vegetation biomass as a parabolic function of inundation level (Kirwan & Murray, 2007; Mariotti & Fagherazzi, 2010). However, a previous study showed that the final equilibrium topographic profiles under SLR are very similar under the linear and non-linear functions (Zhang et al., 2020). Therefore, we only used the linear biomass function here. The details of this model, including the equations of erosion, sedimentation, and vegetation biomass, are provided in D'Alpaos et al. (2007) and Zhang et al. (2020).

An offline coupling approach was used in this study to integrate the Sed model and the SWI model (an online coupling scheme is under development). Specifically, we (a) first simulated the coastal marsh evolution by using the Sed model and (b) used the simulated future surface elevation from step (a) as the initial topographic and morphologic condition to simulate future SWI until equilibrium by using the SWI model.

2.2. Numerical Experiment Design

We designed the synthetic numerical experiments by generalizing marsh landscape features from some real-world coastal marshes, such as the marshlands on the Atlantic coast, where the coastal wetlands are observed and expected to encounter a higher SLR than other US coastal areas (Schieder et al., 2018; Thieler, 2000). Also, these landscapes were identified as topographic limited landscapes which are more sensitive to topographic change and sea level rise (Gleeson et al., 2011; Michael et al., 2013). Specifically, we designed two 2-D synthetic coastal marsh transects that include a 1 m wide coastal marshland (2,000 m long) and an upland region (1,000 m long) (see Figure 1). The transects are perpendicular to shorelines without lateral water flow with adjacent tidal creeks. We assumed that the coastal marshland is covered by salt-tolerant marsh species, such as *Spartina-alterniflora* (Morris et al., 2002). The slope of the coastal marsh (1:2,500) represents an averaged slope of the coastal marsh transects as measured in some Delaware Bay marshlands by this study. The upland slopes of 1:1,000 and 1:250 represent different upland controls on surface-subsurface water propagation and sediment transport (Fagherazzi et al., 2019). We considered a two-layer soil system with a less permeable mud/peat top layer (0 to 5 m) below the ground surface and a high permeable sandy bottom layer (5 to 12 m below the ground surface at the ocean boundary and the thickness slightly increased landward) (Figure 1), which is consistent with previous modeling studies on coastal marshes, such as Xin et al. (2013) and Guimond et al. (2020). Accordingly, we set different soil

Table 1
Key Parameter Values Used in the Numerical Experiments

Parameter	Value	Ref.	Parameter	Value	Ref.
Porosity	0.4 and 0.5 (top and bottom layers)	Guimond et al. (2020)	Hydraulic conductivity (m/day)	0.8 and 8 (top and bottom layers)	Knott et al. (1987); Powers (2020); Ryan (2017)
Manning's n (s $m^{-1/3}$)	0.18	Shih and Rahi (1981)	van Genuchten α for water retention (m^{-1})	1.48 and 2.68 (top and bottom layers)	Guimond et al. (2020)
van Genuchten n for water retention	5.9 and 14.5 (upper and bottom layers)	Guimond et al. (2020)	Residual saturation	0.15 and 0.1 (top and bottom layers)	Guimond et al. (2020)
Saltwater concentration in the ocean (kg salt per kg seawater)	0.0357	Michael et al. (2013)	Suspended sediment concentration in the ocean (mg/L)	50	Kirwan, Walters, et al. (2016)
Erosion coefficient (kg/m^2s)	3×10^{-4}	Fagherazzi and Furbish (2001)	Critical shear stress for erosion (P_a)	0.4	D'Alpaos et al. (2006)
Critical shear stress for deposition (P_a)	0.1	D'Alpaos et al. (2006)	Sediment settling velocity (m/s)	1×10^{-4}	Zhang et al. (2020)
Belowground organic production (m/yr)	0.003	Morris et al. (2016)	Maximum aboveground biomass (g/m^2)	2000	D'Alpaos et al. (2007)
Median particle diameter (m)	5×10^{-5}	D'Alpaos et al. (2007)	z_max (Maximum elevation withstood by marsh plants)	MHTL (mean highest tide level)	D'Alpaos et al. (2007)
z_min (Minimum elevation withstood by marsh plants)	MSL (mean sea level)	D'Alpaos et al. (2007)	Vegetation stem-related parameters	$\alpha_n = 250$ $\beta_n = 0.3032$	D'Alpaos et al. (2007)
Vegetation height-related parameters	$\alpha_h = 0.0609$ $\beta_h = 0.1876$	D'Alpaos et al. (2007)	Vegetation stem diameter-related parameters	$\alpha_d = 0.0006$ $\beta_d = 0.3$	D'Alpaos et al. (2007)

porosities, soil hydraulic conductivity, and van Genuchten water retention parameters for the two layers (see the details of parameter values and references in Table 1).

The land surface hydrodynamics are driven by tides and SLR at the ocean boundary on the right side of the model domain. Initially, the mean sea level (MSL) is equal to 0 m, the same as the elevation of the present-day coastal marsh near the ocean boundary (see Figure 1). To reflect future SLR, we adopted two widely-used future global mean SLR scenarios based on the Representative Concentration Pathways (RCP) 4.5 and RCP 8.5 scenarios in Phase 5 of the Coupled Model Intercomparison Project (CMIP5) (Spencer et al., 2016), including (a) a relatively low SLR rate of 0.5 m/100-year (Da Lio et al., 2013; Ganju et al., 2020; Kirwan & Temmerman, 2009; Sefelnasr & Sherif, 2014; Spencer et al., 2016) and (b) a relatively high SLR rate of 1 m/100-year (Carretero et al., 2013; Langevin & Zygnerski, 2013; Lu et al., 2015; Michael et al., 2013; Sefelnasr & Sherif, 2014; Watson et al., 2010; Yang et al., 2015). We applied a sinusoidal semi-diurnal tide with a tidal range of 1.6 m based on the National Oceanic and Atmospheric Administration (NOAA) tide and current observation at the Delaware Bay, USA (Cape May Station, station ID: 8,536,110). A constant saltwater concentration of 0.0357 (kg salt per kg saltwater) in the ocean (Michael et al., 2013) is set at the ocean boundary.

Freshwater supply comes from the upland, where we assumed a hydrostatic groundwater table (GWT) at the upland boundary (head-controlled boundary condition as introduced in the introduction Section). This study used three upland GWT scenarios to represent (a) a present-day upland GWT condition (1.3 m above the initial MSL), (b) a future GWT condition with increased groundwater extraction and/or a drier climate (0.9 m above the initial MSL), and (c) a future GWT condition with a wetter climate (1.8 m above the initial MSL), respectively. To simplify the control factors and present a more focused study on the effect of marsh evolution on SWI, we did not include the effect of rainfall recharge and evapotranspiration in this study. These effects are discussed in the discussion section and will be explored in future work. We used a head-controlled upland GWT boundary condition, which may predict more SWI than the flux-controlled upland boundary condition for unconfined

Table 2
The Numerical Experiment Cases With Different Upland Slope, SLR, and GWT Scenarios

	Milder upland slope		Steeper upland slope	
	Higher SLR	Lower SLR	Higher SLR	Lower SLR
Medium upland GWT (h = 1.3 m) (present-day scenario)	Case 1	Case 2	Case 3	Case 4
High upland GWT (h = 1.8 m) (wetter climate scenario)	Case 5	Case 6	Case 7	Case 8
Low upland GWT (h = 0.9 m) (drier climate and/or more groundwater extraction scenario)	Case 9	Case 10	Case 11	Case 12

aquifers, according to Werner and Simmons (2009). Therefore, our scenarios may represent a relatively more aggressive prediction of SWI under SLR. All scenarios are summarized in Table 2.

For the eco-geomorphological processes, we simulated surface sediment entrainment, transport, and deposition driven by surface water flow and organic soil production due to vegetation productivity. Sediment fluxes can only flow in and out of the model domain through the ocean boundary, where a constant suspended sediment concentration (50 mg/L) was used at the boundary. The simulations assumed a transport of sediment with a median grain size of 50 μm representing silt as used in a previous coastal eco-geomorphologic modeling study (D'Alpaos et al., 2007). See the parameter details in Table. 1.

The 2-D model domain in Figure 1 was decomposed into a logically structured mesh with a horizontal resolution of ∼5 m and a vertical resolution of ∼1 m (20 layers). We simulated 100-year marsh evolution, and the SWI experiments were simulated until the subsurface salinity reached a dynamic equilibrium state under regular tidal cycles.

2.3. Evaluating the Impact of Marsh Evolution on SWI Under SLR and Tides

We evaluated the effect of marsh evolution on SWI by comparing the SWI simulation with and without marsh evolution under future SLR. Specifically, we created two groups of experiments. Each group consisted of all 12 experimental cases listed in Table. 2. The first group of experiments was based on the present-day marsh topography illustrated in Figure 1. SWI was simulated under future sea level and different upland GWTs without considering coastal marsh evolution. In contrast, the second group conducted the same SWI simulations as in the first group but used the evolved marshland topography in the future 100 years as the topography. With the SLR rates of 0. 5 m/100-year and 1 m/100-year, the future MSL increases to 0.5 and 1 m in 100 years, respectively. Accordingly, the mean highest tide levels (MHTL, equal to MSL + tidal amplitude) rise from 0.8 to 1.3 m and 1.8 m, respectively. We examined the surface and subsurface freshwater and saltwater changes in the two groups of numerical experiments. Specifically, we analyzed the changes in surface seawater propagation, inflow, concentration, and infiltration and subsurface water salinity, seawater inflow, and the displacement of the freshwater-seawater interface.

3. Results

3.1. Coastal Marsh Evolution Driven by Tidal and SLR Forcing

Driven by the future SLR, our modeling results showed that the marsh elevation rises substantially with SLR and with a larger increase near the ocean boundary and a smaller increase for the inland marsh (Figures 2a and 2b) due to a gradient in sedimentation rates (Figure 3). Therefore, a topographic depression forms in the middle of the marshland. The future elevations near the ocean boundary are close to the future MHTLs under both the higher and lower SLR rates. Correspondingly, the vegetation co-evolves with the topographic change and future inundation conditions. The salt-tolerant vegetation biomass is modeled to increase linearly with inundation level, which results in higher vegetation biomass in the middle of the domain due to a higher inundation level (MHTL minus the elevation in the middle of the domain) and lower vegetation biomass at the ocean and upland sides because of lower inundation levels (Figures 2c and 2d). Relative to the initial marshland (the gray dashed lines in Figures 2c and 2d; 1,000–3,000m from the upland boundary), there is a landward expansion of marsh vegetation that varied with SLR and upland slopes. For example, the marsh vegetation covers the entire upland region in the case with the milder slope and higher SLR rate (the light green line in Figure 2c) because the future MHTL (1.8 m) is the

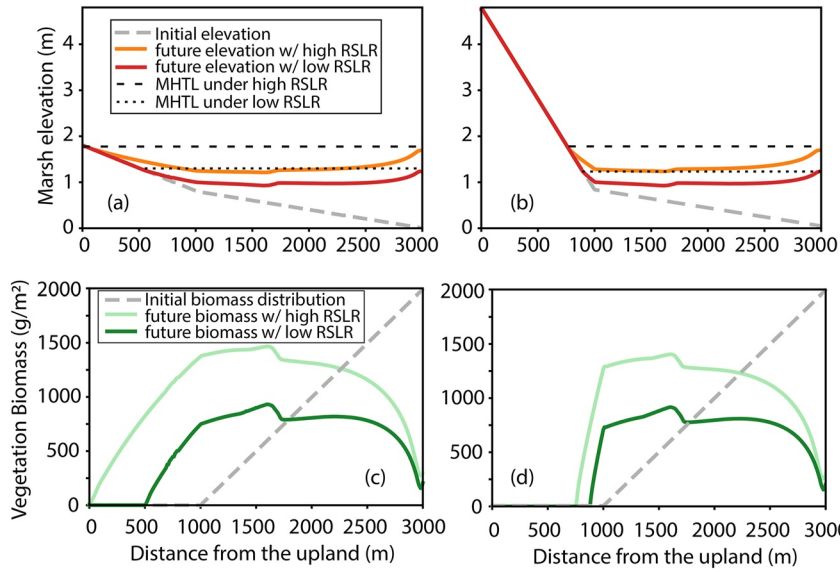

Figure 2. The distribution of future elevation and vegetation biomass of the domain with a milder upland slope (a and c) and a steeper upland slope (b and d). The gray dashed lines indicate the initial surface elevation and vegetation biomass distribution, respectively. MHTL stands for the mean highest tide level. RSLR is the rate of sea level rise.

same as the elevation of the upland boundary leading to an inundation condition favorable for vegetation growth. For the cases with the steeper upland slope, a large portion of the upland areas is still higher than the MHTL, therefore no vegetation presents in the upland areas (Figure 2d).

Among sedimentation rates across the domain, the largest spatial variation comes from the sediment settling rate (the light blue lines in Figure 3), which is the greatest near the ocean boundary because of higher sediment input from the ocean and decreases landward, due to a declined sediment supply from the ocean. The spatial variation of sediment settling rate primarily contributes to the spatial variation of the evolved topography. The vegetation organic matter production rate slightly varies across the domain with a higher rate in the middle of

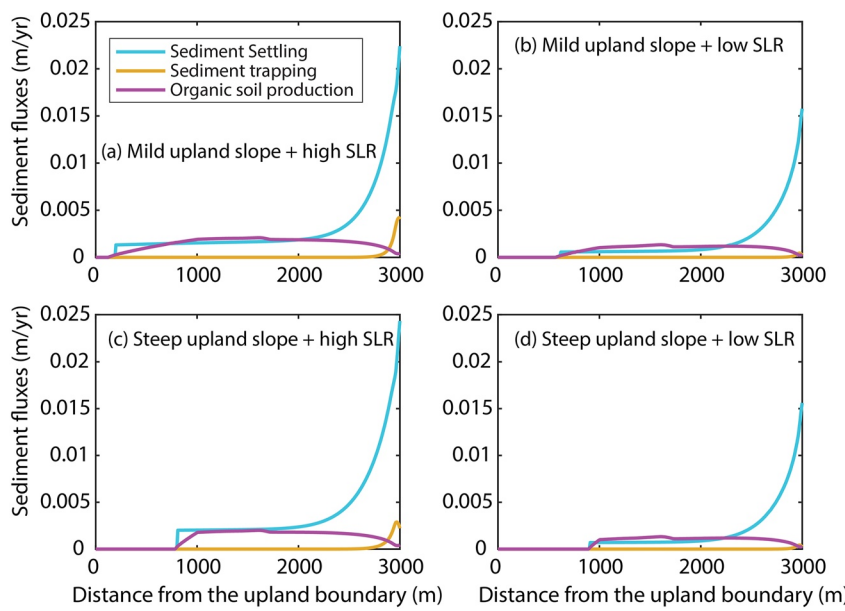

Figure 3. The spatial distribution of the sediment fluxes at the end of the 100-year simulation. The plots with various colors represent different fluxes in different scenarios.

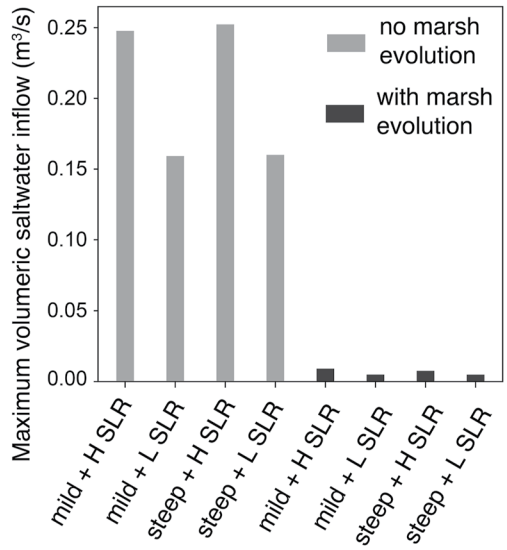

Figure 4. The maximum seawater inflows under future sea level for the simulations with and without considering coastal marsh evolution. The gray and black bars indicate the simulated seawater inflow without and with considering marsh evolution, respectively.

the domain due to higher vegetation biomass (the purple lines in Figure 3). Vegetation sediment trapping contributed the least to the landscape accretion as the trapping rate is relatively low, compared to the sediment settling rate and vegetation organic production rate. The trapping rate is high near the ocean boundary where the sediment concentration and flow velocity are higher (flow velocity distributions during a high tide and low tide and sediment concentration are given in Figures S3, S4, and S5). Moving landward, the trapping effect vanishes very quickly due to the decrease in sediment concentration and flow velocity (the yellow lines in Figure 3). We included the sediment erosion process in the model simulation. However, sediment erosion is only observed at the beginning of the simulation when the future SLR is suddenly applied to the domain boundary (not shown). Later in the simulation, the erosion rate drops to zero because (a) the marsh vegetation attenuates water flow and the bed shear stress is too small, compared with the critical shear stress, to cause erosion and (b) the water flow rate decreases at the ocean boundary because the increased elevation makes the hydraulic gradient smaller between the land and the ocean.

3.2. SWI With and Without Marsh Evolution

3.2.1. The Influence of Marsh Evolution on Coastal Hydrodynamics

After predicting the topographic change of the coastal marsh landscapes 100 years in the future, we compared the SWI under SLR with and without considering marsh evolution. Take the cases with the present-day upland GWT (1.3 m) as an example, without considering marsh topographic change in the future 100 years, the rising sea level increases the hydraulic gradient between the ocean and the marshland, thus more saltwater was predicted to flow onto the marshland with a relatively larger maximum inflow rate (~0.25 m^3/s) under the higher SLR scenario and a relatively lower rate (~0.16 m^3/s) under the lower SLR scenario (the Gy bars in Figure 4), compared to the maximum rate of 0.1 m^3/s under the present-day condition (not shown). However, considering marsh evolution (e.g., Figures 2a and 2b), the hydraulic gradient between the ocean and the marshland decreases. Thus, the saltwater maximum inflows are predicted to be ~0.009 m^3/s for the higher SLR rate scenario and ~0.0048 m^3/s for the lower SLR rate scenario (the black bars in Figure 4). These rates are two orders of magnitude smaller than the maximum rates in the cases without considering marsh evolution.

The marsh topographic change also affects surface seawater propagation, ponding water depth, surface water residence time, and saltwater concentration on the marsh surface. Figure 5 shows the maximum surface water propagation and associated surface saltwater concentration for the cases without considering marsh evolution (the top four plots with gray backgrounds) and with marsh evolution (the bottom four plots with white backgrounds). Without considering marsh evolution, seawater propagates landward during the high tides and causes a surface inundation with a maximum inundation depth higher than 1.3 m near the ocean boundary (the yellow solid lines in Figures 5a–5c and 5d). During the high tides, the saltwater concentration in the ponded water is close to the concentration in the ocean (3.5%; the blue dashed lines in Figures 5a–5c and 5d). During the low tides, the surface ponding water flows out from the marsh domain (the yellow dashed lines in Figures 5a–5c and 5d). Therefore, the residence time for surface saltwater is tightly controlled by the tidal frequency.

In contrast, considering marsh evolution 100 years in the future, the future sea level and tides are not applied to a static marsh landscape, but to an evolved marsh landscape with an increased elevation throughout the domain due to sedimentation. This evolved marsh landscape significantly changes seawater inflow and propagation on the land surface. Saltwater flows onto the marshland during the high tides with a much smaller inflow rate due to a smaller hydraulic gradient as illustrated in Figure 4, and then the saltwater gradually accumulates in the evolved depression zone in the middle of the marshland barely flowing out from the domain during the low tides, which largely increases the residence time of saltwater (the yellow solid and dashed lines in Figures 5e–5h). Meanwhile, more upland freshwater can accumulate in the depression zone through subsurface freshwater exfiltration, diluting the saltwater concentration in the depression zone. Thus, we see a higher saltwater concentration near the ocean side due to more saltwater inputs from the ocean and a lower concentration inland because the saltwater

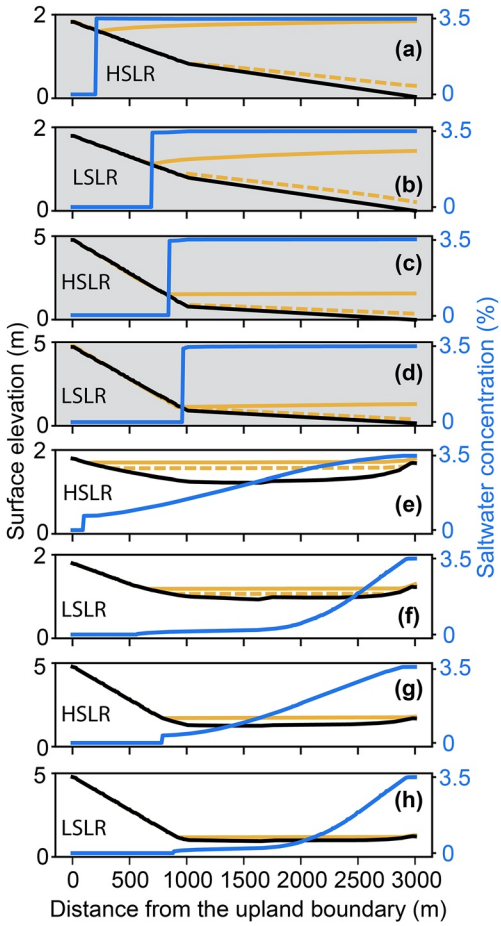

Figure 5. The surface water propagation and associated surface water concentration in the simulations with and without the considerations of marsh topographic change. (a), (b), (c), and (d) with the gray background are the cases without considering marsh evolution. (e), (f), (g), and (h) are the cases considering marsh evolution. The black solid lines are the surface elevation. The yellow solid and dashed lines indicate the maximum and minimum surface water propagation under the high and low tides, respectively. The blue lines indicate the distribution of the saltwater concentration under the maximum surface water propagation conditions. HSLR and LSLR stand for the higher and lower SLR rate scenarios, respectively.

mixes with more freshwater from the upland, compared to the cases without marsh evolution. However, the distribution of saltwater concentration also varies under different SLR rates. For example, in the cases with a higher SLR rate (Figures 5e and 5g), the upland GWT (=1.3 m) is lower than the future MHTL (=1.8 m). Due to a smaller hydraulic gradient between the freshwater GWT and the sea level, less fresh groundwater flows into the marsh aquifer. Thus, at a dynamic equilibrium state, the surface saltwater concentration is higher than the concentration in the case under a lower SLR rate (Figures 5f and 5h), where the upland GWT (1.3 m) is at the same level as the future MHTL (1.3 m) and the fresh groundwater can be more easily flowing into the marsh aquifer to dilute saltwater.

3.2.2. Subsurface Salinity Distribution

Under the present-day condition (upland GWT = 1.3 m and MSL = 0 m) without SLR, Figures 6a and 6b show the dynamic equilibrium of the salinity distribution in the aquifer with milder and steeper upland slopes, respectively. The toes and heads of the freshwater-saltwater interfaces (the white dashed lines) are at ~1,000 and ~1,500 m from the upland boundary, respectively. Starting from this present-day equilibrium condition, we applied the new sea level in the future 100 years to the model domain to simulate future SWI. For the cases without considering marsh evolution (Figures 6c–6f), we predicted an increase of SWI with the increase of future sea level. The increases in SWI are attributed to the SLR-induced surface saltwater infiltration and subsurface lateral saltwater inflow. With the increased sea level, more surface areas are inundated during the high tides, which results in more seawater infiltrating to the subsurface aquifer. Meanwhile, more seawater flows into the aquifer directly through the subsurface lateral flow due to the increased hydraulic gradient between the sea level and the inland water table. We analyzed the changes in surface saltwater infiltration and subsurface lateral inflows from the beginning of the simulation to the final equilibrium state (see Figure S6 and Text S2). In general, the surface saltwater infiltration contributed less to the subsurface SWI than the subsurface lateral inflow (see the blue solid lines in Figure S6) primarily because saltwater cannot infiltrate to the subsurface as easily through the less permeable top layer as the subsurface seawater can flow laterally through the subsurface high permeable sandy layer. The different upland slopes also affect saltwater intrusion by changing surface saltwater propagation. For example, we observed a lower salinity near the upper part of the aquifer in the cases with a steeper upland slope, where the surface saltwater cannot propagate to the upland boundary during the high tides (Figures 6d and 6f).

In contrast, when marsh evolution was considered, under the higher SLR rate, the freshwater-saltwater interfaces almost reach the upland boundary (Figures 6g and 6h), similar to the simulations without marsh evolution. This is because the subsurface lateral seawater inflow still contributes, and dominates, the landward intrusion of seawater, especially for the lower part of the aquifer. The subsurface lateral seawater inflow is barely affected by the surface topographic change. The second reason is that, although the surface saltwater inflow is low (Figure 4), the surface depression zone accumulates seawater and prolongs the time of surface saltwater infiltration contributing to the salinity increase of the upper aquifer. However, under the lower SLR rate, as we showed in Subsection 3.2.1 above, surface water salinity largely decreases because more upland freshwater can enter the domain and dilute saltwater due to a lower hydraulic gradient between the sea level and the upland GWT (the blue lines in Figures 5f and 5h). Therefore, the low surface salinity limits saltwater infiltration, and we see a distinct subsurface saltwater distribution: the toe of the freshwater-saltwater interface moves toward the upland boundary, but the head of the interface near the marsh surface moves toward the ocean boundary. More freshwater occupies the upper part of the aquifer in the middle of the marshland (Figures 5i and 5j).

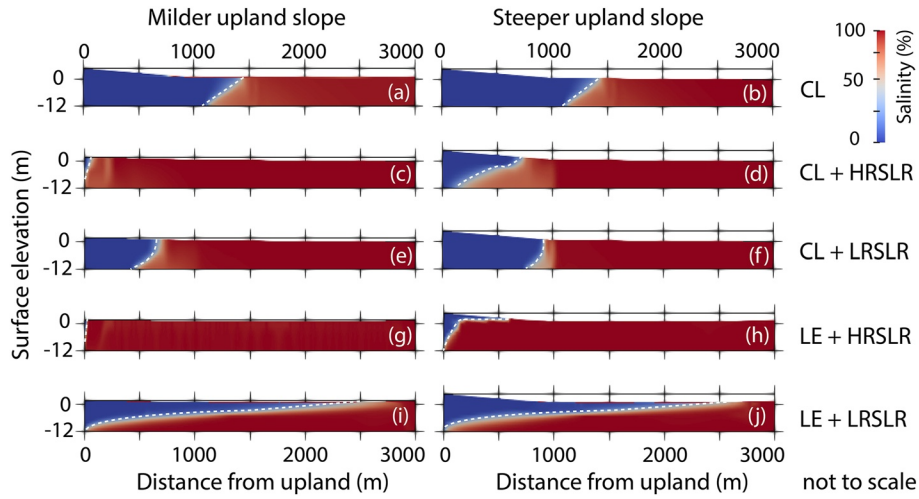

Figure 6. The distribution of subsurface saltwater concentration under the present-day sea level (a) and (b), future sea level (c,d, e, and f), and future sea level and topographic change (g, h, i, and j). All the simulations are under the present-day upland ground water table of 1.3 m. The left and right columns are the simulations with the milder and steeper upland slopes, respectively. The white dashed lines indicate the locations of the freshwater-saltwater interfaces.

3.3. SWI Under Different Upland GWT Levels

With future climate change, the upland GWT condition may also change. Therefore, we also investigated the future SWI in response to different future upland GWT conditions: (a) a higher upland GWT due to a wetter future climate and (b) a lower GWT due to a drier future climate or a higher upland groundwater extraction (cases 5 to 12 in Table 2). With the same model settings and same SLR rate scenarios, a higher upland GWT (1.8 m above the initial MSL) causes a larger hydraulic gradient toward the ocean, thereby more freshwater flows the upland boundary into the aquifer. Therefore, the simulations predict a lower SWI for all cases under the high upland GWT (Figure 7), compared with the cases under the present-day upland GWT (Figure 6). In particular, the cases with marsh evolution show a larger decrease of SWI at the upper aquifer (Figures 7g and 7h), compared with the corresponding cases under the present-day upland GWT (Figures 6g and 6h). This is because the higher groundwater head can provide more fresh groundwater from the upland and better counteract the saltwater intrusion.

However, a lower upland GWT (0.9 m above the initial MSL) creates a larger hydraulic gradient toward the land, causing more saltwater flows onto the marsh surface and into the aquifer. Therefore, more SWIs are observed in all simulation cases with the lower future upland GWT (Figure 8). In particular, we see a larger increase of SWI for the cases with the marsh evolution and under the lower SLR rate (Figures 8i and 8j), compared with the corresponding cases under the present-day upland GWT in Figures 6i and 6j. This is because the upland groundwater supply is not sufficient to counteract the saltwater inflow on the surface and in the aquifer, which results in more saltwater infiltration and subsurface lateral saltwater inflow.

4. Discussion

4.1. Marsh Evolution and Its Representativeness

The eco-geomorphologic simulations above showed that coastal marsh landscapes are not static, but dynamic in response to future sea level rise. Under the external drivers of SLR and tidal current, coastal marsh elevation is very likely to increase and can keep pace with future SLR rates due to sedimentation. Although the future marsh topographies predicted by our study are the results of the combined effect of the specific tidal amplitude, SLR rates, sediment concentration in the ocean, tidal period, and sediment diffusivity, the predicted marsh accretion is consistent with many coastal marshes at the Atlantic and Gulf Coasts in North America and Europe (Kirwan, Temmerman, et al., 2016). The measured accretion rates of these coastal marshes, especially the low marshes, can keep pace with SLR rates ranging from 2 mm/yr to 10 mm/yr (Kirwan, Temmerman, et al., 2016). The dynamic eco-geomorphologic feedback to SLR described in the Sed model is the key to their survival (see

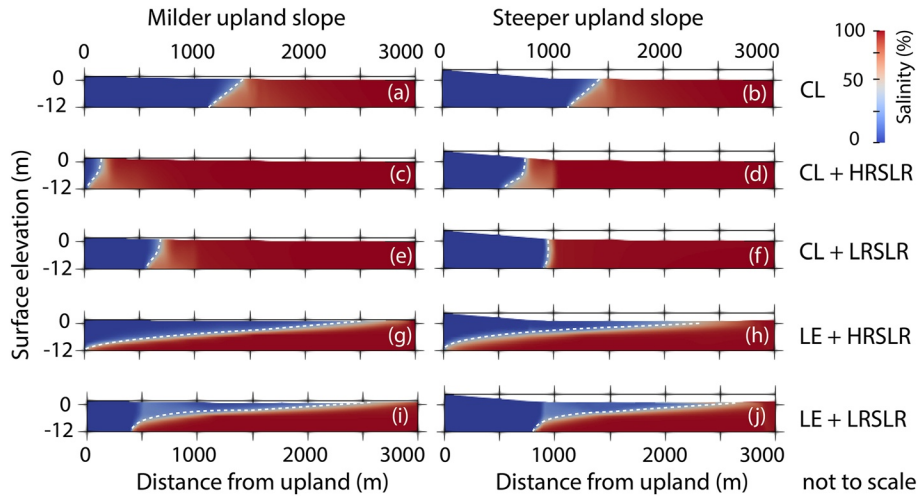

Figure 7. The distribution of subsurface saltwater concentration under the present-day sea level (a) and (b), future sea level (c,d, e, and f), and future sea level and topographic change (g, h, i, and j). All the simulation results are under the upland ground water table of 1.8 m. The left and right columns are the simulations with the milder and steeper upland slopes, respectively. The white dashed lines indicate the locations of the freshwater-saltwater interfaces.

Subsection 2.1.2). The model parameters used in this study were established in the literature from field measurements (Fagherazzi et al., 2013; Kirwan, Temmerman, et al., 2016; Morris et al., 2002; Mudd et al., 2004) and reflect real-world coastal marsh landscapes.

We also predicted the spatial variation of marsh accretion and found that the coastal marsh accretion rate is very likely to be higher near the ocean boundary than in the middle of the domain due to a gradient in the sedimentation rates, which is consistent with previous predictions (e.g., Kirwan, Walters, et al., 2016; Zhang et al., 2020). Notably, because of the decline of sediment input landward, the sediment settling rate and sediment trapping rate due to vegetation are small (e.g., the middle of the domain in Figure 3). Vegetation organic matter production is critical in contributing to the elevation increase in the middle of the marshland. We predicted that the marsh vegetation biomass may be higher in the depression zone due to a higher inundation level. Notably, a longer duration of inundation in the depression zone will increase the toxicity of the soil, which may result in the mortality of marsh vegetation (Pennings et al., 2005; Pezeshki, 1998, 2001; Visser & Sandy, 2009). Although this effect is

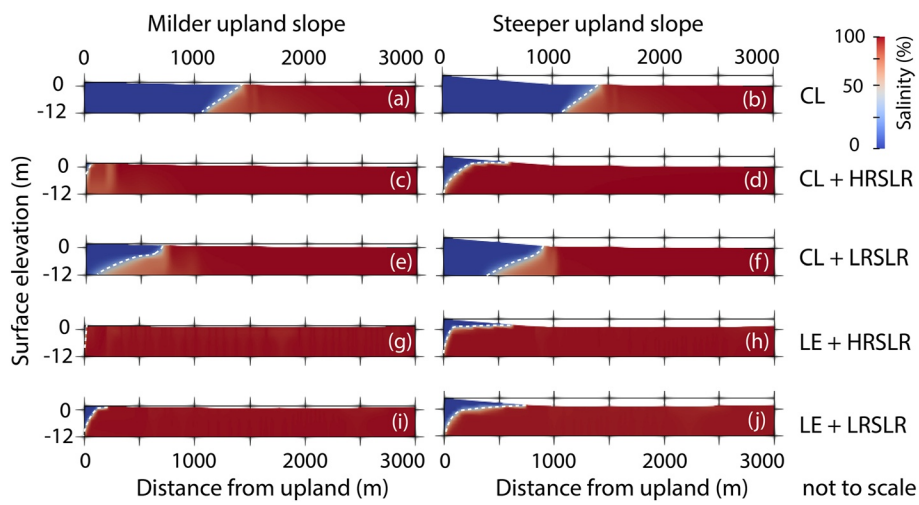

Figure 8. The distribution of subsurface saltwater concentration under the present-day sea level (a) and (b), future sea level (c,d, e, and f), and future sea level and topographic change (g, h, i, and j). All the simulation results are under the upland groundwater table of 0.9 m. The left and right columns are the simulations with the milder and steeper upland slopes, respectively. The white dashed lines indicate the locations of the freshwater-saltwater interfaces.

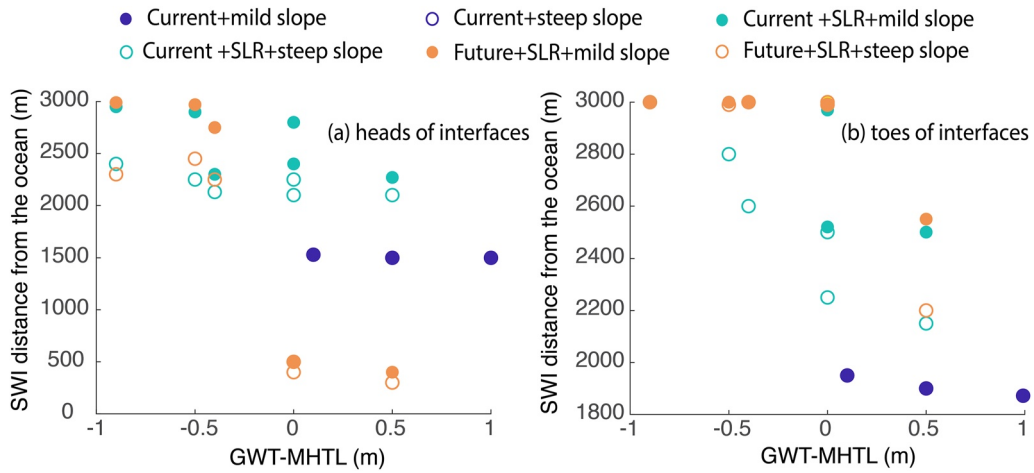

Figure 9. Saltwater intrusion distance as a function of ground water table -mean highest tide level (GWT-MHTL) under different sea level rise scenarios and upland slopes. (a) is the distance between the head of the interface and the ocean boundary and (b) is the distance between the toe of the interface and the ocean boundary. The terms, "current" and "future" in the legend, stand for current landscape topography and future marsh topography after marsh evolution. The circles and dots indicate the simulations under the milder and steeper upland slopes, respectively. Note the blue circles and dots are overlapped when GWT-MHTL >0, so the blue circles are not visible.

not included in this study, if we consider the long-time inundation effect on vegetation growth, the contribution of vegetation organic soil production to sedimentation will be decreased due to lower vegetation productivity, which will enlarge the elevation relief between the boundary and the middle of the domain. Therefore, we may expect an even deeper depression zone.

4.2. Effect of Coastal Marsh Evolution on Coastal SWI

The evolved marsh landscape under future SLR has an important influence on coastal SWI, especially on the saltwater surface inflow, surface saltwater residence time, and saltwater infiltration. First, the future evolved marsh topography significantly reduces the seawater inflow on the marsh surface because the increased marsh elevation near the ocean boundary reduces the hydraulic gradient between the marshland and the ocean. The predicted surface seawater inflow can be up to two orders of magnitude smaller than the inflow without considering marsh evolution implying that the seawater inflow may be overestimated in the studies that do not consider marsh evolution (e.g., the saltwater inflows in Figure 3). Second, the depression zone formed during the marsh evolution processes can accumulate both seawater and freshwater, which significantly increases the surface water residence time on the marsh surface and prolongs infiltration time. These modeling results are consistent with Yu et al. (2016), where they assessed the role of surface depression in controlling water flow path and seawater infiltration under storm surge inundation. Therefore, marsh topographic change can result in a very different hydrologic regime, compared with the predictions without considering marsh evolution as we demonstrated above (e.g., Figures 4–6, and S6).

The model results also suggest that the upland GWT effect is more significant under an evolving marsh landscape because the exfiltrated freshwater from the upland remains longer in the surface depression zone to counteract the surface saltwater inflow. For example, the cases with marsh evolution show larger variations in the displacements of the freshwater-saltwater interface with the different upland GWTs (e.g., Figures 6–8). By compiling all the cases with the different upland GWTs in Figures 6–8, we found that the difference between the upland GWT and MHTL (GWT-MHTL) is a good metric to understand the effect of marsh evolution on SWI under future SLR. Specifically, Figure 9 shows the displacements of the heads and toes of the freshwater-saltwater interfaces as a function of GWT-MHTL based on the cases in Figures 6–8. We found that the toes of the interfaces in the cases considering marsh evolution reach similar locations to the corresponding cases without marsh evolution (Figure 9a). However, the heads of the interfaces present a larger difference over the cases. When GWT-MHTL is greater than zero (a hydraulic gradient toward the ocean), we found that the cases considering marsh evolution exhibit the shortest distance between the head of the interface and the ocean boundary. However, if GWT-MHTL

is less than zero (a hydraulic gradient toward the inland), the difference between the heads of the interfaces is very small between the cases with and without marsh evolution (the orange dots and circles in Figure 9b). Therefore, the difference in the displacement of the interface reveals that marsh evolution may increase the sensitivity of the marsh system to the future upland GWT conditions, highlighting the importance of protecting upland groundwater resources to prevent intensified SWI in the future.

These results have important real-world implications. The topographic change of these coastal marshes at the decadal to century scales may have an important influence on the land-ocean interaction and may not be ignored in predicting future SWI. For example, when predicting future SLR-induced SWI on coastal marshes, like the marshlands in the Atlantic and Gulf Coasts in North America and Europe mentioned above, their increased elevation can significantly change the hydrologic regimes and the temporal and spatial distribution of SWI.

4.3. The Influence of Future SWI on Vegetation Dynamics

The eco-geomorphologic impact on SWI also has important ecological implications. Subsurface water salinity has a direct impact on vegetation growth, species richness, species distribution, and migration (Antonellini & Mollema, 2010; Silvestri & Marani, 2004). In previous studies that did not consider marsh evolution, the subsurface SWI was predicted to occupy a larger area of the coastal aquifers under SLR (e.g., Kuan et al., 2012; Michael et al., 2013), which may exert larger stress on vegetation growth. Therefore, the retreat rate of forests and farmlands are expected to increase. However, our experiments show that the subsurface salinity is very likely to decrease, especially for the upper part of the aquifer with sufficient upland freshwater supply and moderate SLR conditions (e.g., Figs. 6i and j and Figs. 7g, h, i and j). Therefore, the surface ponded freshwater dilutes saltwater providing a different saline condition for vegetation growth, which indicates that the vegetation biomass, species, or distribution may be very different from the previous studies without considering marshland evolution. With the decrease of saltwater intrusion, we also expect that the rate of marsh landward retreat would slow down, reducing the rate of upland forest degradation.

4.4. Uncertainties and Future Work

In this study, we chose to focus on sea level, tide, upland groundwater table, and topographic change, which we felt were critical to our analysis of the coastal eco-geomorphologic impact on SWI. However, several factors may affect the SWI prediction, such as the vegetation dynamic representation, precipitation, evaporation, waves, subsidence, and the land-river-ocean interaction. Specifically, our marsh evolution simulation assumed a linear relationship between the *S.-alterniflora* dominant vegetation biomass and the coastal inundation level based on the field observation by Morris et al. (2002). However, there are other schemes to represent the relationship between vegetation biomass and inundation level for different marsh landscapes, such as the *Spartina*-nonlinear function (Mariotti & Fagherazzi, 2010) and mixed vegetation species linear function (D'Alpaos et al., 2007). Zhang et al. (2020) evaluated the topographic outcomes from these three vegetation schemes and found that all of the schemes predicted a higher elevation increase near the ocean boundary and a lower increase landward. However, these schemes also showed differences in marsh elevation relief and unvegetated-vegetated ratio. Therefore, it is worth exploring SWI under future topographic change with different vegetation dynamic representations. Moreover, the impact of salinity change on vegetation dynamics is not well incorporated in the current coastal eco-geomorphologic models. Our ongoing development of a physically-based vegetation dynamic configuration on ATS will better link surface and subsurface water conditions, including salinity, soil moisture, nutrient content, and inundation level, with vegetation growth.

Precipitation and evaporation may also affect surface and subsurface saltwater transport and distribution (Geng et al., 2016; Morris, 1995; Payne, 2010; Wang et al., 2007; Werner & Simmons, 2009; Xin et al., 2022). We acknowledge that precipitation and evaporation would play an important role in changing water salinity on the land surface and in the upper subsurface zone. For example, precipitation may dilute saltwater and ET may concentrate the water salinity, especially for the surficial soil layer. However, to conduct this focused study, we reduced the complexity by limiting external drivers. We think this is a very important first step. In this way, we can see the impact of eco-geomorphologic change on SWI more clearly and exclusively. The findings of this study would not change with the inclusion of ET and precipitation. Specifically, we found

that the surface seawater inflow is very likely to decrease due to marshland accretion. ET and precipitation have a very limited influence on marsh accretion and seawater inflow because the inflow is driven by the tidal variation, and sediment transport is primarily driven by tidal water flow, not precipitation and ET. The feedback of vegetation productivity due to ET and precipitation-indued salinity change is not included in the current model. The vegetation dynamics in the current model are only driven by the elevation difference between sea level and land elevation. Therefore, including ET and precipitation would not change our findings of the eco-geomorphologic impact on seawater inflow. Additionally, we found that the evolved depression zone in the middle of the marsh landscapes can help accumulate water and prolong water residence time. This geomorphologic impact would not change with ET and precipitation. We note that ET and precipitation influence subsurface salinity mostly during low tide periods, where almost no surface ponding water is present (Geng et al., 2016; Xin et al., 2017). However, in our case, surface ponding water with a depth from ~0.1 to ~0.35 m (see Figures 5e–5g and 5h) can cover most of the marshland. Therefore, the direct rainfall infiltration and soil surface evaporation are very limited. We acknowledge that the specific value of salinity in the surface ponding water may be different with the consideration of ET and precipitation. However, with the continuous seawater input from the ocean, we expect that there is no significant change in the salinity of surface ponded water. The salinity may be very different under some extreme events, but that is out of the scope of this study and worth exploring in future studies.

Additionally, we did not consider erosion due to waves because marsh vegetation can mitigate waves if the waves are caused by the regular tidal variation and wind speed (D'Alpaos et al., 2007; Marani et al., 2007). However, some evidence also showed that salt marsh may not be able to prevent wetland edge erosion depending on variable soil types (Feagin et al., 2009). In particular, under climatic extreme events, like hurricanes and storm surges, the large waves may not be effectively mitigated by the marsh vegetation, and marshland erosion may occur and exceed the rate of sediment deposition. In this case, marsh elevation may decrease, especially near the ocean boundary as predicted by Mariotti and Fagherazzi (2010). The decrease in marsh elevation may increase surface saltwater inflow, thereby stimulating SWI. Also, hurricanes may directly cause distinct surface and subsurface water salinity distribution due to a dramatic increase in seawater level (Yu et al., 2016). Although it is not the scope of this study, it is worth exploring the effect of marsh evolution on SWI under these extreme climatic events in future studies. Another important process is coastal subsidence as it causes the elevation decline of coastal marshlands. There are multiple reasons for coastal subsidence, such as groundwater extraction, soil consolidation, and organic matter decomposition (Cahoon & Lynch, 1997; Hatton et al., 1983; Yu & Michael, 2019; Zoccarato et al., 2019). It is worth exploring how these factors would impact coastal subsidence to provide a more accurate prediction of coastal morphological change in future studies.

Lastly, this study used transects that do not allow for surface water drainage paths connecting the marshland and marsh drainage network, which may facilitate the drainage of the surface ponding water to channels and increase sediment input to the inland marshlands. This will require a 2-D simulation that captures the complex topography of marshes with channels and drainage pathways. Also, the role of 3-D hydrodynamics is not considered and worthy of additional future study as it would incorporate baroclinic effects that can contribute to tidally-driven sedimentation. We used the diffusive-wave scheme to estimate water flow, where Manning's coefficient was used to represent the drag effect of vegetation on water flow. There are many other ways to estimate vegetation drag effect on flow by considering detailed 1-D or 2-D vegetation structures, such as vegetation stem diameter, stem density, and vegetation height (Mudd et al., 2004). Cao et al. (2021) made a comprehensive comparison between different methods for drag coefficient parameterization, including Manning's coefficient approach. This detailed water flow estimation is out of the scope of this study but is worth exploring in future studies.

One challenge of conducting this type of study comes from the lack of field measurement data for validating both the eco-geomorphologic processes and subsurface salinity at the same marsh location. However, this limitation also brings an opportunity for future studies to enhance field measurement to better support SWI studies where the eco-geomorphologic impact is also involved. The model results in this study can help inform future field measurement plans. For example, planning field measurements on a site with both hydrological and geomorphological importance would be more useful to understand future saltwater intrusion of real-world marshes.

5. Conclusions

In this study, we investigated the impact of coastal marsh evolution on SWI prediction under future SLR by using a physically-based coastal hydro-eco-geomorphologic model, ATS (Advanced Terrestrial Simulator). Using a generalized coastal marsh landscape, we first predicted the marsh landscape change with different upland slopes and under two SLR scenarios. We found that the coastal marsh landscape is not static but dynamic in response to SLR. The marsh elevation increases with the rising sea level due to the organic and inorganic sedimentation and created a higher elevation near the ocean boundary and a depression zone in the middle of the marshland. The marsh accretion is projected to cause a significant reduction of saltwater inflow at the ocean boundary because of the decrease in the hydraulic gradient between the land and ocean. Also, the evolved topographic depression zone prolongs the residence time of surface ponding water, which affects surface saltwater infiltration, therefore causing distinct subsurface salinity distributions. With the evolved marsh landscape, we also tested the impact of different upland groundwater conditions on SWI under SLR, reflecting the impact of future drier/wetter climate conditions and human groundwater extraction on fresh groundwater dynamics. We found that with the topographic change in the future, SWI is more sensitive to the upland fresh groundwater supply because of the intensified freshwater-saltwater interaction in the depression zone. Therefore, when predicting future SWI on coastal marsh landscape, if we do not consider marsh evolution, we are very likely to overestimate SWI under future SLR if the upland GWT is higher than the MHTL, whereas we may underestimate SWI if the future upland GWT is lower than the MHTL.

This study highlighted the importance of considering coastal marsh landscape change in predicting SWI under SLR, which was not investigated in previous studies. Over the decadal and century scales, changes in coastal landscape topography can significantly affect the temporal and spatial distributions of SWI under SLR. The insights gained from this study can help improve our understanding of the vulnerability of coastal freshwater systems under SLR, marsh landscape dynamics, and changes in upland groundwater resources, where these interconnections have been previously ignored but warrant greater consideration.

Data Availability Statement

This study is a model-based study that uses the ATS model and synthetic experiments. The model-related files are available at ESS-DIVE (https://data.ess-dive.lbl.gov/data) with project name of "ats morphologic and saltwater intrusion simulations."

Acknowledgments
We acknowledge the constructive comments from Dr. Julia Guimond and the other two anonymous reviewers. We also thank Dr. Pei Xin's lab-experiment data for validating the saltwater intrusion benchmark simulations in this study. The research presented in this paper was supported by the Laboratory Direct Research and Development (LDRD) program at Los Alamos National Laboratory (LANL) under project number 20180033DR. The paper revision was supported by the Environmental System Science (ESS) program areas of the U.S. Department of Energy, Office of Science, Office of Biological and Environmental Research as part of the multi-program, collaborative Integrated Coastal Modeling (ICoM) project. This study was also partially supported by the Center for Space and Earth Sciences (CSES) Rapid Response Project at LANL under project number 20210528CR. This research used resources provided by the Los Alamos National Laboratory Institutional Computing Program, which is supported by the U.S. Department of Energy National Nuclear Security Administration under Contract No. 89233218CNA000001.

References

Antonellini, M., & Mollema, P. N. (2010). Impact of groundwater salinity on vegetation species richness in the coastal pine forests and wetlands of Ravenna, Italy. *Ecological Engineering*, *36*(9), 1201–1211. https://doi.org/10.1016/j.ecoleng.2009.12.007

Ataie-Ashtiani, B., Werner, A. D., Simmons, C. T., Morgan, L. K., & Lu, C. (2013). How important is the impact of land-surface inundation on seawater intrusion caused by sea-level rise? *Hydrogeology Journal*, *21*(7), 1673–1677. https://doi.org/10.1007/s10040-013-1021-0

Belliard, J.-P., Toffolon, M., Carniello, L., & D'Alpaos, A. (2015). An ecogeomorphic model of tidal channel initiation and elaboration in progressive marsh accretional contexts. *Journal of Geophysical Research: Earth Surface*, *120*(6), 1040–1064. https://doi.org/10.1002/2015JF003445

Best, Ü. S. N., Van der Wegen, M., Dijkstra, J., Willemsen, P. W. J. M., Borsje, B. W., & Roelvink, D. J. A. (2018). Do salt marshes survive sea level rise? Modelling wave action, morphodynamics and vegetation dynamics. *Environmental Modelling & Software*, *109*, 152–166. https://doi.org/10.1016/j.envsoft.2018.08.004

Burkett, V., & Kusler, J. (2000). *Climate change: Potential impacts and Interactions in Wetlands ofF the United States*.

Cahoon, D. R., & Lynch, J. C. (1997). Vertical accretion and shallow subsidence in a mangrove forest of southwestern Florida, U.S.A. *Mangroves and Salt Marshes*, *1*(3), 173–186. https://doi.org/10.1023/A:1009904816246

Cao, Z., Zhang, Y., Wolfram, P. J., Brus, S. R., Rowland, J. C., Xu, C., et al. (2021). Effects of different vegetation drag parameterizations on the tidal propagation in coastal marshlands. *Journal of Hydrology*, *603*, 126775. https://doi.org/10.1016/j.jhydrol.2021.126775

Carretero, S., Rapaglia, J., Bokuniewicz, H., & Kruse, E. (2013). Impact of sea-level rise on saltwater intrusion length into the coastal aquifer, Partido de La Costa, Argentina. *Continental Shelf Research*, *61–62*, 62–70. https://doi.org/10.1016/j.csr.2013.04.029

Chang, S. W., Clement, T. P., Simpson, M. J., & Lee, K.-K. (2011). Does sea-level rise have an impact on saltwater intrusion? *Advances in Water Resources*, *34*(10), 1283–1291. https://doi.org/10.1016/j.advwatres.2011.06.006

Chen, W.-B., Liu, W.-C., & Hsu, M.-H. (2015). Modeling assessment of a saltwater intrusion and a transport time scale response to sea-level rise in a tidal estuary. *Environmental Fluid Mechanics*, *15*(3), 491–514. https://doi.org/10.1007/s10652-014-9367-y

Coon, E. T., David Moulton, J., & Painter, S. L. (2016). Managing complexity in simulations of land surface and near-surface processes. *Environmental Modelling & Software*, *78*, 134–149. https://doi.org/10.1016/j.envsoft.2015.12.017

Da Lio, C., D'Alpaos, A., & Marani, M. (2013). The secret gardener: Vegetation and the emergence of biogeomorphic patterns in tidal environments. *Philosophical Transactions of the Royal Society A: Mathematical, Physical & Engineering Sciences*, *371*(2004), 20120367. https://doi.org/10.1098/rsta.2012.0367

D'Alpaos, A., Lanzoni, S., Mudd, S. M., & Fagherazzi, S. (2006). Modeling the influence of hydroperiod and vegetation on the cross-sectional formation of tidal channels. *Estuarine, Coastal and Shelf Science*, *69*(3), 311–324. https://doi.org/10.1016/j.ecss.2006.05.002

D'Alpaos, A., Marani, M., & Rinaldo, A. (2007). Landscape evolution in tidal embayments: Modeling the interplay of erosion, sedimentation, and vegetation dynamics. *Journal of Geophysical Research*, *112*(F1). https://doi.org/10.1029/2006JF000537

Fagherazzi, S., Anisfeld, S. C., Blum, L., Long, E. V., Feagin, R. A., Fernandes, A., et al. (2019). Sea level rise and the dynamics of the marsh-upland boundary. *Frontiers in Environmental Science*, *7*. https://doi.org/10.3389/fenvs.2019.00025

Fagherazzi, S., FitzGerald, D., Fulweiler, R., Hughes, Z., Wiberg, P., McGlathery, K., et al. (2013). *Ecogeomorphology of salt marshes*.

Fagherazzi, S., & Furbish, D. J. (2001). On the shape and widening of salt marsh creeks. *Journal of Geophysical Research*, *106*(C1), 991–1003. https://doi.org/10.1029/1999JC000115

Feagin, R. A., Lozada-Bernard, S. M., Ravens, T. M., Möller, I., Yeager, K. M., & Baird, A. H. (2009). Does vegetation prevent wave erosion of salt marsh edges? *Proceedings of the National Academy of Sciences*, *106*(25), 10109–10113. https://doi.org/10.1073/pnas.0901297106

Ferguson, G., & Gleeson, T. (2012). Vulnerability of coastal aquifers to groundwater use and climate change. *Nature Climate Change*, *2*(5), 342–345. https://doi.org/10.1038/nclimate1413

Ganju, N. K., Defne, Z., & Fagherazzi, S. (2020). Are elevation and open-water conversion of salt marshes connected? *Geophysical Research Letters*, *47*(3), e2019GL086703. https://doi.org/10.1029/2019GL086703

Geng, X., Boufadel, M. C., & Jackson, N. L. (2016). Evidence of salt accumulation in beach intertidal zone due to evaporation. *Scientific Reports*, *6*(1), 31486. https://doi.org/10.1038/srep31486

Giambastiani, B. M. S., Antonellini, M., Oude Essink, G., & Stuurman, R. (2007). Saltwater intrusion in the unconfined coastal aquifer of Ravenna (Italy): A numerical model. *Journal of Hydrology*, *340*(1–2), 91–104. https://doi.org/10.1016/j.jhydrol.2007.04.001

Gleeson, T., Marklund, L., Smith, L., & Manning, A. H. (2011). Classifying the water table at regional to continental scales. *Geophysical Research Letters*, *38*(5). https://doi.org/10.1029/2010gl046427

Guimond, J., & Tamborski, J. (2021). Salt marsh hydrogeology: A eview. *Water*, *13*(4), 543. https://doi.org/10.3390/w13040543

Guimond, J., Yu, X., Seyfferth, A. L., & Michael, H. A. (2020). Using hydrological-biogeochemical linkages to elucidate carbon dynamics in coastal marshes subject to relative sea level rise. *Water Resources Research*, *56*(2), e2019WR026302. https://doi.org/10.1029/2019WR026302

Hatton, R. S., DeLaune, R. D., & Patrick, W. H., Jr. (1983). Sedimentation, accretion, and subsidence in marshes of Barataria Basin, Louisiana1. *Limnology & Oceanography*, *28*(3), 494–502. https://doi.org/10.4319/lo.1983.28.3.0494

Herbert, A. W., Jackson, C. P., & Lever, D. A. (1988). Coupled groundwater flow and solute transport with fluid density strongly dependent upon concentration. *Water Resources Research*, *24*(10), 1781–1795. https://doi.org/10.1029/WR024i010p01781

Hughes, J. D., Vacher, H. L., & Sanford, W. E. (2009). Temporal response of hydraulic head, temperature, and chloride concentrations to sea-level changes, Floridan aquifer system, USA. *Hydrogeology Journal*, *17*(4), 793–815. https://doi.org/10.1007/s10040-008-0412-0

Ketabchi, H., Mahmoodzadeh, D., Ataie-Ashtiani, B., Werner, A. D., & Simmons, C. T. (2014). Sea-level rise impact on fresh groundwater lenses in two-layer small islands. *Hydrological Processes*, *28*(24), 5938–5953. https://doi.org/10.1002/hyp.10059

Kirwan, M., & Murray, A. B. (2007). A coupled geomorphic and ecological model of tidal marsh evolution. *Proceedings of the National Academy of Sciences*, *104*(15), 6118–6122. https://doi.org/10.1073/pnas.0700958104

Kirwan, M., & Temmerman, S. (2009). Coastal marsh response to historical and future sea-level acceleration. *Quaternary Science Reviews*, *28*(17), 1801–1808. https://doi.org/10.1016/j.quascirev.2009.02.022

Kirwan, M., Temmerman, S., Skeehan, E. E., Guntenspergen, G. R., & Fagherazzi, S. (2016). Overestimation of marsh vulnerability to sea level rise. *Nature Climate Change*, *6*(3), 253–260. https://doi.org/10.1038/nclimate2909

Kirwan, M., Walters, D. C., Reay, W. G., & Carr, J. A. (2016). Sea level driven marsh expansion in a coupled model of marsh erosion and migration. *Geophysical Research Letters*, *43*(9), 4366–4373. https://doi.org/10.1002/2016GL068507

Knott, J. F., Nuttle, W. K., & Hemond, H. F. (1987). Hydrologic parameters of salt marsh peat. *Hydrological Processes*, *1*(2), 211–220. https://doi.org/10.1002/hyp.3360010208

Kuan, W. K., Jin, G., Xin, P., Robinson, C., Gibbes, B., & Li, L. (2012). Tidal influence on seawater intrusion in unconfined coastal aquifers. *Water Resources Research*, *48*(2). https://doi.org/10.1029/2011WR010678

Kuan, W. K., Xin, P., Jin, G., Robinson, C. E., Gibbes, B., & Li, L. (2019). Combined effect of tides and varying inland groundwater input on flow and salinity distribution in unconfined coastal aquifers. *Water Resources Research*, *55*(11), 8864–8880. https://doi.org/10.1029/2018WR024492

Langevin, C. D., & Zygnerski, M. (2013). Effect of sea-level rise on salt water intrusion near a coastal well field in Southeastern Florida. *Groundwater*, *51*(5), 781–803. https://doi.org/10.1111/j.1745-6584.2012.01008.x

Loáiciga, H. A., Pingel, T. J., & Garcia, E. S. (2012). Sea water intrusion by sea-level rise: Scenarios for the 21st century. *Groundwater*, *50*(1), 37–47. https://doi.org/10.1111/j.1745-6584.2011.00800.x

Lu, C., Xin, P., Li, L., & Luo, J. (2015). Seawater intrusion in response to sea-level rise in a coastal aquifer with a general-head inland boundary. *Journal of Hydrology*, *522*, 135–140. https://doi.org/10.1016/j.jhydrol.2014.12.053

Marani, M., D'Alpaos, A., Lanzoni, S., Carniello, L., & Rinaldo, A. (2007). Biologically-controlled multiple equilibria of tidal landforms and the fate of the Venice lagoon. *Geophysical Research Letters*, *34*(11). https://doi.org/10.1029/2007gl030178

Mariotti, G., & Fagherazzi, S. (2010). A numerical model for the coupled long-term evolution of salt marshes and tidal flats. *Journal of Geophysical Research*, *115*(F1). https://doi.org/10.1029/2009JF001326

Masterson, J. P., & Garabedian, S. P. (2007). Effects of sea-level rise on ground water flow in a coastal aquifer system. *Groundwater*, *45*(2), 209–217. https://doi.org/10.1111/j.1745-6584.2006.00279.x

Mazi, K., Koussis, A. D., & Destouni, G. (2013). Tipping points for seawater intrusion in coastal aquifers under rising sea level. *Environmental Research Letters*, *8*(1), 014001. https://doi.org/10.1088/1748-9326/8/1/014001

Michael, H. A., Russoniello, C. J., & Byron, L. A. (2013). Global assessment of vulnerability to sea-level rise in topography-limited and recharge-limited coastal groundwater systems. *Water Resources Research*, *49*(4), 2228–2240. https://doi.org/10.1002/wrcr.20213

Morgan, L. K., Stoeckl, L., Werner, A. D., & Post, V. E. A. (2013). An assessment of seawater intrusion overshoot using physical and numerical modeling. *Water Resources Research*, *49*(10), 6522–6526. https://doi.org/10.1002/wrcr.20526

Morris, J. T. (1995). The mass balance of salt and water in intertidal sediments: Results from North Inlet, South Carolina. *Estuaries*, *18*(4), 556–567. https://doi.org/10.2307/1352376

Morris, J. T., Barber, D. C., Callaway, J. C., Chambers, R., Hagen, S. C., Hopkinson, C. S., et al. (2016). Contributions of organic and inorganic matter to sediment volume and accretion in tidal wetlands at steady state. *Earth's Future*, *4*(4), 110–121. https://doi.org/10.1002/2015EF000334

Morris, J. T., Sundareshwar, P., Nietch, C. T., Kjerfve, B., & Cahoon, D. R. (2002). Responses of coastal wetlands to rising sea level. *Ecology*, *83*(10), 2869–2877. https://doi.org/10.1890/0012-9658(2002)083[2869:rocwtr]2.0.co;2

Mudd, S. M., Fagherazzi, S., Morris, J. T., & Furbish, D. J. (2004). Flow, sedimentation, and biomass production on a vegetated salt marsh in South Carolina: Toward a predictive model of marsh morphologic and ecologic evolution. *The Ecogeomorphology of Tidal Marshes, Coastal Estuarine Stud*, *59*, 165–187.

Oude Essink, G., Van Baaren, E. S., & De Louw, P. G. (2010). Effects of climate change on coastal groundwater systems: A modeling study in the Netherlands. *Water Resources Research*, *46*(10). https://doi.org/10.1029/2009wr008719
Payne, D. F. (2010). Effects of sea-level rise and pumpage elimination on saltwater intrusion in the Hilton Head Island Area, South Carolina, 2004—2104. *U.S. Geological Survey Scientific Investigations Report 2009–*, *5251*, 83.
Pennings, S. C., Grant, M.-B., & Bertness, M. D. (2005). Plant zonation in low-latitude salt marshes: Disentangling the roles of flooding, salinity and competition. *Journal of Ecology*, *93*(1), 159–167. https://doi.org/10.1111/j.1365-2745.2004.00959.x
Pezeshki, S. R. (1998). Photosynthesis and root growth in Spartina alterniflora in relation to root zone aeration. *Photosynthetica*, *34*(1), 107–114. https://doi.org/10.1023/A:1006820019220
Pezeshki, S. R. (2001). Wetland plant responses to soil flooding. *Environmental and Experimental Botany*, *46*(3), 299–312. https://doi.org/10.1016/S0098-8472(01)00107-1
Powers, M. (2020). *Tidal-groundwater study of the Slaughter Beach salt marsh in Slaughter Beach*. DE. West Chester University Master's Theses. Retrieved from https://digitalcommons.wcupa.edu/all_theses/125
Rasmussen, P., Sonnenborg, T. O., Goncear, G., & Hinsby, K. (2013). Assessing impacts of climate change, sea level rise, and drainage canals on saltwater intrusion to coastal aquifer. *Hydrology and Earth System Sciences*, *17*(1), 421–443. https://doi.org/10.5194/hess-17-421-2013
Richards, L. A. (1931). Capillary conduction of liquids through porous mediums. *Physics*, *1*(5), 318–333. https://doi.org/10.1063/1.1745010
Ryan, C. (2017). *Subsurface Transport in a North inlet, South Carolina salt marsh: A Porewater salinity model* (Bachelor of Science). University of South Carolina. Retrieved from https://www.proquest.com/openview/c1918d5b2acd1d92ee7029e8bbb0c977/1?pq-origsite=gscholar&cbl=18750
Schieder, N., Walters, D., & Kirwan, M. (2018). Massive upland to wetland conversion compensated for historical marsh loss in Chesapeake Bay, USA. *Estuaries and Coasts*, *41*(4), 940–951. https://doi.org/10.1007/s12237-017-0336-9
Sefelnasr, A., & Sherif, M. (2014). Impacts of seawater rise on seawater intrusion in the Nile Delta aquifer, Egypt. *Groundwater*, *52*(2), 264–276. https://doi.org/10.1111/gwat.12058
Shih, S. F., & Rahi, G. S. (1981). Seasonal variations of Manning's roughness coefficient in a subtropical marsh. *Transaction of the ASAE*, *25*(1), 116–119.
Silvestri, S., & Marani, M. (2004). Salt-marsh vegetation and morphology: Basic physiology, modelling and remote sensing observations. *The Ecogeomorphology of Tidal Marshes, Coastal Estuarine Stud*, *59*, 5–25.
Simmons, C. T., Fenstemaker, T. R., & Sharp, J. M. (2001). Variable-density groundwater flow and solute transport in heterogeneous porous media: Approaches, resolutions and future challenges. *Journal of Contaminant Hydrology*, *52*(1), 245–275. https://doi.org/10.1016/S0169-7722(01)00160-7
Sorensen, R. M., Weisman, R. N., & Lennon, G. P. (1984). Control of erosion, inundation, and salinity intrusion caused by sea level rise. In M. C. Barth, & J. G. Titus (Eds.), *Greenhouse effect and sea level rise* (pp. 179–214). Springer US. https://doi.org/10.1007/978-1-4684-6569-3_6
Sousa, A. I., Lillebø, A. I., Pardal, M. A., & Caçador, I. (2010). Productivity and nutrient cycling in salt marshes: Contribution to ecosystem health. *Estuarine, Coastal and Shelf Science*, *87*(4), 640–646. https://doi.org/10.1016/j.ecss.2010.03.007
Spencer, T., Schuerch, M., Nicholls, R. J., Hinkel, J., Lincke, D., Vafeidis, A. T., et al. (2016). Global coastal wetland change under sea-level rise and related stresses: The DIVA Wetland Change Model. *Global and Planetary Change*, *139*, 15–30. https://doi.org/10.1016/j.gloplacha.2015.12.018
Thieler, E. R. (2000). *National Assessment of Coastal Vulnerability to Future Sea-Level Rise* (No. 076–00). *Fact Sheet. U.S. Geological Survey*. https://doi.org/10.3133/fs07600
Tiner, R. W. (2013). *Tidal wetlands primer*. University of Massachusetts Press.
Vandenbohede, A., Luyten, K., & Lebbe, L. (2008). Effects of global change on heterogeneous coastal aquifers: A case study in Belgium. *Journal of Coastal Research*, *24*(sp2), 160–170. https://doi.org/10.2112/05-0447.1
Visser, J., & Sandy, E. (2009). The effects of flooding on four common Louisiana Marsh Plants. *Gulf of Mexico Science*, *27*(1). https://doi.org/10.18785/goms.2701.03
Vreugdenhil, C. B. (1994). Shallow-water flows. In C. B. Vreugdenhil (Ed.), *Numerical methods for Shallow-water flow* (pp. 1–14). Springer Netherlands. https://doi.org/10.1007/978-94-015-8354-1_1
Vu, D. T., Yamada, T., & Ishidaira, H. (2018). Assessing the impact of sea level rise due to climate change on seawater intrusion in Mekong Delta, Vietnam. *Water Science and Technology*, *77*(6), 1632–1639. https://doi.org/10.2166/wst.2018.038
Wang, H., Hsieh, Y. P., Harwell, M. A., & Huang, W. (2007). Modeling soil salinity distribution along topographic gradients in tidal salt marshes in Atlantic and Gulf coastal regions. *Ecological Modelling*, *201*(3), 429–439. https://doi.org/10.1016/j.ecolmodel.2006.10.013
Watson, T. A., Werner, A. D., & Simmons, C. T. (2010). Transience of seawater intrusion in response to sea level rise. *Water Resources Research*, *46*(12). https://doi.org/10.1029/2010WR009564
Werner, A. D., & Simmons, C. T. (2009). Impact of sea-level rise on sea water intrusion in coastal aquifers. *Groundwater*, *47*(2), 197–204. https://doi.org/10.1111/j.1745-6584.2008.00535.x
Werner, A. D., Ward, J. D., Morgan, L. K., Simmons, C. T., Robinson, N. I., & Teubner, M. D. (2012). Vulnerability indicators of sea water intrusion. *Groundwater*, *50*(1), 48–58. https://doi.org/10.1111/j.1745-6584.2011.00817.x
Winn, K. O., Saynor, M. J., Eliot, M. J., & Elio, I. (2006). Saltwater intrusion and morphological change at the mouth of the East Alligator River, Northern Territory. *Journal of Coastal Research*, *2006*(221), 137–149. https://doi.org/10.2112/05A-0011.1
Xin, P., Li, L., & Barry, D. A. (2013). Tidal influence on soil conditions in an intertidal creek-marsh system. *Water Resources Research*, *49*(1), 137–150. https://doi.org/10.1029/2012WR012290
Xin, P., Wilson, A., Shen, C., Ge, Z., Moffett, K. B., Santos, I. R., et al. (2022). Surface water and groundwater interactions in salt marshes and their impact on plant ecology and coastal biogeochemistry. *Reviews of Geophysics*, *60*(1), e2021RG000740. https://doi.org/10.1029/2021RG000740
Xin, P., Zhou, T., Lu, C., Shen, C., Zhang, C., D'Alpaos, A., & Li, L. (2017). Combined effects of tides, evaporation and rainfall on the soil conditions in an intertidal creek-marsh system. *Advances in Water Resources*, *103*, 1–15. https://doi.org/10.1016/j.advwatres.2017.02.014
Yang, J., Graf, T., & Ptak, T. (2015). Sea level rise and storm surge effects in a coastal heterogeneous aquifer: A 2D modelling study in northern Germany. *Grundwasser*, *20*(1), 39–51. https://doi.org/10.1007/s00767-014-0279-z
Yu, X., & Michael, H. A. (2019). Offshore pumping impacts onshore groundwater resources and land subsidence. *Geophysical Research Letters*, *46*(5), 2553–2562. https://doi.org/10.1029/2019GL081910
Yu, X., Yang, J., Graf, T., Koneshloo, M., O'Neal, M. A., & Michael, H. A. (2016). Impact of topography on groundwater salinization due to ocean surge inundation. *Water Resources Research*, *52*(8), 5794–5812. https://doi.org/10.1002/2016WR018814
Zhang, Y., Li, W., Sun, G., & King, J. S. (2019). Coastal wetland resilience to climate variability: A hydrologic perspective. *Journal of Hydrology*, *568*, 275–284. https://doi.org/10.1016/j.jhydrol.2018.10.048

Zhang, Y., Li, W., Sun, G., Miao, G., Noormets, A., Emanuel, R., & King, J. S. (2018). Understanding coastal wetland hydrology with a new regional-scale, process-based hydrological model. *Hydrological Processes*, *32*(20), 3158–3173. https://doi.org/10.1002/hyp.13247

Zhang, Y., Rowland, J. C., Xu, C., Wolfram, P. J., Svyatsky, D., Moulton, J. D., et al. (2020). Understanding the eco-geomorphologic feedback of coastal marsh under sea level rise: Vegetation dynamic representations, processes interaction, and parametric sensitivity. *Journal of Geophysical Research: Earth Surface*, *125*(11), e2020JF005729. https://doi.org/10.1029/2020JF005729

Zoccarato, C., Lio, C. D., Tosi, L., & Teatini, P. (2019). A coupled biomorpho-geomechanical model of tidal marsh evolution. *Water Resources Research*, *55*(11), 8330–8349. https://doi.org/10.1029/2019WR024875